A prominent pattern of year-to-year variability in Indian Summer Monsoon Rainfall

Vimal Mishra[a,1], Brian V. Smoliak[b], Dennis P. Lettenmaier[a], and John M. Wallace[b]

[a]Civil and Environmental Engineering and [b]Atmospheric Sciences, University of Washington, Seattle, WA 98195

Edited by Robert E. Dickinson, University of Texas, Austin, TX, and approved March 28, 2012 (received for review November 21, 2011)

The dominant patterns of Indian Summer Monsoon Rainfall (ISMR) and their relationships with the sea surface temperature and 850-hPa wind fields are examined using gridded datasets from 1900 on. The two leading empirical orthogonal functions (EOFs) of ISMR over India are used as basis functions for elucidating these relationships. EOF1 is highly correlated with all India rainfall and El Niño–Southern Oscillation indices. EOF2 involves rainfall anomalies of opposing polarity over the Gangetic Plain and peninsular India. The spatial pattern of the trends in ISMR from 1950 on shows drying over the Gangetic Plain projects onto EOF2, with an expansion coefficient that exhibits a pronounced trend during this period. EOF2 is coupled with the dominant pattern of sea surface temperature variability over the Indian Ocean sector, which involves in-phase fluctuations over the Arabian Sea, the Bay of Bengal, and the South China Sea, and it is correlated with the previous winter's El Niño–Southern Oscillation indices. The circulation anomalies observed in association with fluctuations in the time-varying indices of EOF1 and EOF2 both involve distortions of the low-level monsoon flow. EOF1 in its positive polarity represents a southward deflection of moist, westerly monsoon flow from the Arabian Sea across India, resulting in a smaller flux of moisture to the Himalayas. EOF2 in its positive polarity represents a weakening of the monsoon trough over northeastern India and the westerly monsoon flow across southern India, reminiscent of the circulation anomalies observed during break periods within the monsoon season.

The importance of Indian Summer Monsoon Rainfall (ISMR) for agricultural production, water availability, and food security is well-documented (1). Interannual monsoon variability strongly affects agricultural production, which accounts for about 22% of the Indian gross domestic product (2). Disruptions in the ISMR can lead to substantial losses in crop production that, in turn, may affect the food security of the large and growing population of India.

July through September ISMR averaged over the entire Indian subcontinent is remarkably steady from one year to the next, with a coefficient of variation of only 9%. However, even these small variations have important consequences for food production. Rainfall over India as a whole is known to be negatively correlated with sea surface temperature (SST) anomalies over the equatorial eastern Pacific Ocean: it tends to be enhanced during the cold years and suppressed during the warm years of the El Niño–Southern Oscillation (ENSO) cycle (2–9). Rainfall during the monsoon season over India has also been linked with SST variability in the Indian Ocean: the Indian Ocean Dipole mode (10, 11) and a more general warming (cooling) of the tropical Indian Ocean during El Niño (La Niña) events through the so-called atmospheric bridge that persists into the following summer (12–14).

Here, we identify a prominent pattern of year-to-year ISMR variability in which the anomalies exhibit a dipole structure with anomalies of opposing sign over the Gangetic Plain and peninsular India. The accompanying low-level wind anomalies project strongly onto the climatological mean summer monsoon circulation; positive anomalies, as defined here, denote a weakening of the low-level westerly monsoon flow across peninsular India and vice versa. We show the existence of this dipole pattern in ISMR, and we show that it is related to a well-defined pattern of SST anomalies over the Arabian Sea, the Bay of Bengal, and the South China Sea, reminiscent of the lagged response to the ENSO cycle. We also describe the related structures in the wind and geopotential height fields. In *Discussion*, we offer a dynamical interpretation of these observational results, and in *Materials and Methods*, we summarize our results and comment on the use of linear analysis techniques such as empirical orthogonal function (EOF) analysis in the study of ISMR.

SST and Rainfall Patterns

We first consider the preferred patterns of summer monsoon rainfall anomalies over India on a year-to-year basis and their relationship with global SST anomalies. When maximal covariance analysis (MCA) is performed using the raw SST field, the global warming trend influences the structure of the leading modes. Because the emphasis in this study is on SST gradients rather than SST itself, the analysis is performed on the SST departure field (i.e., the departure of SST in each grid cell in each year's monsoon season from the globally averaged SST for that season). We have verified that transforming the SST field in this way simplifies the structure of the leading MCA modes.

Fig. 1 shows the relationship between monsoon season rainfall over India and SST variability based on MCA performed separately on global SST and SST over the Indian Ocean sector for the period of record from 1900 to 2008. The leading mode based on the SST departure field in the global domain, which accounts for 79.4% of the squared covariance between the two fields (Fig. 1*A*), resembles the characteristic signature of ENSO. The corresponding anomalies in ISMR (Fig. 1*B*) are of opposite sign of the SST anomalies over the equatorial eastern Pacific. Hence, in agreement with previous studies cited in the Introduction, we find that ISMR tends to be generally suppressed when SST over the tropical eastern Pacific is anomalously high (i.e., during El Niño years).

The second mode of the MCA, which accounts for 14% of the squared covariance (almost three-quarters of the residual squared covariance after the first mode is removed), involves a pattern of SST anomalies with centers of action of like sign over the northern Arabian Sea, the Bay of Bengal, and the South China Sea (Fig. 1*C*) coupled with a north–south dipole in ISMR (Fig. 1*D*). Above normal SST in these regions is observed in association with below normal rainfall in the Gangetic Plain region and above normal rainfall over peninsular India to the east of the Ghats (Fig. 1*D*). The SST patterns for both modes exhibit weaker features over the Atlantic sector, which we disregard in this paper. In both the first and second modes, the correlation

Author contributions: V.M. and J.M.W. designed research; V.M. performed research; V.M., B.V.S., and J.M.W. analyzed data; and V.M., D.P.L., and J.M.W. wrote the paper.

The authors declare no conflict of interest.

This article is a PNAS Direct Submission.

[1]To whom correspondence should be addressed. E-mail: vmishra@hydro.washington.edu.

This article contains supporting information online at www.pnas.org/lookup/suppl/doi:10.1073/pnas.1119150109/-/DCSupplemental.

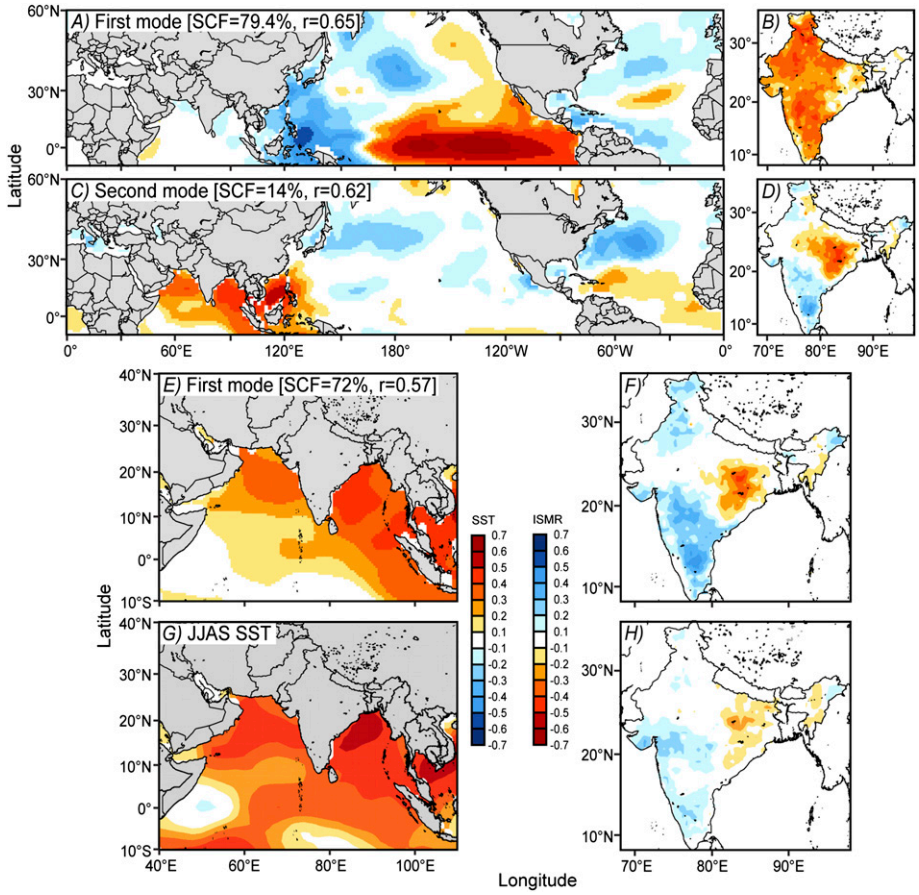

Fig. 1. Coupled patterns of SST and JJAS ISMR variability estimated by performing MCA on the 109-y record from 1900 to 2008. The analysis is based on the SST departure field defined as the departure of each year's SST anomaly at each grid point from that year's global mean SST anomaly. The patterns indicated by colored shading are the heterogeneous correlation coefficients between the ISMR expansion coefficient time series and the SST departure field at each grid point and vice versa. The (dimensionless) scale is indicated in the color bar. (*A–D*) Leading two modes for the global SST domain. (*E* and *F*) Leading mode for the tropical Indian Ocean SST sector. (*G*) Correlation between monsoon season SST departure field and previous winter's (November to January) Nino 3.4 index. (*H*) Same as *G* but for ISMR. The squared covariance fraction (SCF) and temporal correlation between the SST and ISMR expansion coefficients (*r*) are indicated at the top in *A*, *C*, and *E*.

coefficients between the SST and ISMR expansion coefficients are highly significant.

To verify the reality of the second mode in the above MCA expansion, we repeat the MCA on Indian Ocean SST (40° E to 110° E and 10° S to 40° N) and ISMR. The leading mode (Fig. 1 *E* and *F*) closely resembles the second mode obtained in the global SST expansion (Fig. 1 *C* and *D*); it accounts for 72% of the squared covariance in this regional domain, and its SST and ISMR expansion coefficients are highly correlated. Hence, when ISMR is considered in relation to SST variations over the Indian Ocean sector alone, the leading mode of variability is virtually identical to the second mode derived from the MCA with the global SST departure field.

To investigate the patterns of ISMR variability without reference to SST, we perform EOF analysis on the standardized ISMR field (Fig. 2). The values that are plotted can either be viewed as regression coefficients of standardized rainfall on the standardized principle components (PCs) or simply, correlation coefficients. The two leading EOFs account for 20% and 9% of the variance, respectively. EOF1 strongly resembles the ISMR pattern in leading MCA mode, in which ISMR is paired with the global SST departure field (Fig. 1*B*). EOF2 resembles the pattern in the second mode (Fig. 1*D*), and it also resembles the pattern in the leading mode in MCA for the Indian Ocean sector (Fig. 1*F*). These results indicate the existence of a robust pattern of variability in ISMR that has shown a consistent relationship with Indian Ocean SSTs (Fig. 1 *C* and *E*) in a record extending back over a century. The same patterns emerge when the analysis is performed on the period of record from 1950 to 2008. The PC of the second mode obtained in the EOF analysis (Fig. 2*C*) is negatively correlated with Gangetic Plain rainfall anomalies (Fig. 2*C*) ($r = -0.58$, $P = 0.007$), whereas PC1 of ISMR is strongly correlated with rainfall averaged over India as a whole, referred to as the all-India rainfall index ($r = 0.94$, $P < 0.001$) (15).

Maps of seasonally averaged June to September (JJAS) rainfall over the Indian Ocean sector based on the Global Precipitation Climatology Project (GPCP) data regressed on PC1 and PC2 of ISMR are shown in Fig. 3. The region in which rainfall oscillates in phase with PC1 encompasses almost all of India, Pakistan, and most of the Arabian Sea and the Bay of Bengal. The dipole in ISMR associated with EOF2 (Fig. 2*B*) is seen to be part of a broader northeast–southwest dipole that encompasses large areas of the surrounding seas (Fig. 3*C*).

Related Variability in the Lower Tropospheric Circulation

Here, we document the variations in the wind and geopotential height fields associated with the leading EOFs of ISMR shown in Fig. 2. Fig. 4 *A* and *B* show the climatological mean 850-hPa wind and geopotential height fields during the monsoon season (JJAS)

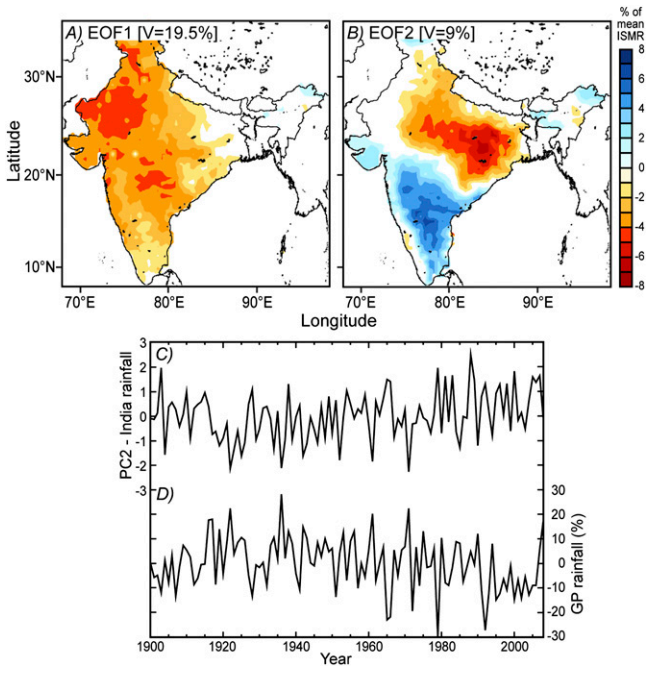

Fig. 2. (*A* and *B*) The two leading EOFs of JJAS ISMR variability for the 109-y period from 1900 to 2008. Shading indicates the rainfall anomalies, expressed as a percentage of the climatological mean ISMR, observed in association with a PC amplitude of +1 SD. V indicates the fraction of the domain-integrated variance explained by the two modes. (*C*) The standardized PC2 (the time series of the expansion coefficient of EOF2) and (*D*) monsoon season rainfall averaged over the Gangetic Plain (21° N to 30° N, 75° E to 89° E) expressed as a percentage of the climatological mean rainfall.

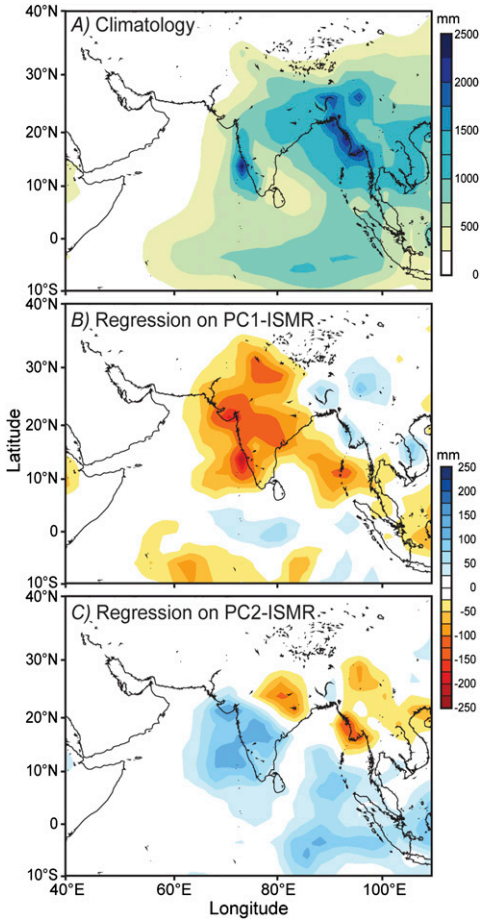

Fig. 3. (*A*) Seasonally averaged JJAS rainfall climatology (millimeters) based on the GPCP dataset for the 30-y period from 1979 to 2008. (*B* and *C*) GPCP summer rainfall regressed on standardized PC1 and PC2 of ISMR, respectively (i.e., standardized time series of the expansion coefficients of the two leading EOFs of ISMR shown in Fig. 2 *A* and *B*).

over India. The broad westerly monsoon flow stretches from the Horn of Africa to Indochina, crossing peninsular India along the southern flank of the monsoon trough that stretches across northern India along the foot of the Himalayas. The patterns derived by regressing those fields on PC1 and PC2 of ISMR are shown in Fig. 4 *C–F*. Positive excursions in PC1 are associated with a weakening of the westerly monsoon flow into India from the Arabian Sea. The anomalous weak flow circulates anticyclonically around the center of the positive 850-hPa height anomalies over northwest India, and on close inspection, it seems to be weakly divergent. The prevalence of positive bias of the 850-hPa height anomalies over the Indian Ocean sector as a whole in Fig. 4*D* is an integral part of the signature of the Southern Oscillation; the Southern Oscillation Index, defined as the difference between the standardized sea level pressure (SLP) anomalies Darwin and Tahiti, is positively correlated with PC1 of ISMR ($r = 0.52$, $P < 0.01$). In fact, the work by Walker (16) used Bombay SLP as an alternative to Darwin SLP in an effort to extend the analysis of the Southern Oscillation back to the 19th century.

The positive polarity of PC2 of ISMR is associated with an anomalous flow pattern indicative of a weakening of the climatological mean westerly low-level monsoon flow farther to the east than the region affected by PC1 (i.e., from the eastern Arabian Sea eastward across India, the Bay of Bengal, and Indochina) (Fig. 4*E*). The corresponding geopotential height pattern shown in Fig. 4*F* is dominated by a band of positive anomalies extending from Indochina northwestward across much of northern India. The wind and height patterns associated with PC2 are geostrophically consistent and indicative of a weakening of the climatological mean monsoon trough and westerly flow along the southern flank of it. They are reminiscent of the patterns observed in association with the so-called break phase of the monsoon (5). The weakening of the monsoon trough is consistent with negative rainfall anomalies over the Gangetic Plain (Fig. 2*B*) and parts of Indochina (Fig. 3*C*).

The positive rainfall anomalies over southern India observed in association with the positive polarity of PC2 (Figs. 2*B* and 3*C*) are consistent with convergence of the low-level wind anomalies over that region (Fig. 4*E*). If only ISMR, as depicted in Fig. 2*B*, were considered, one might be tempted to attribute the positive rainfall anomalies over peninsular India to the east of the Ghats to a weakening of the rain shadow downstream of the Ghats. However, a weakening of the westerlies would not explain the positive rainfall anomalies upwind of the Ghats and offshore in the Arabian Sea (Fig. 3*C*), which seem to be associated with a broad region of anomalous low-level convergence.

Regression patterns very similar to those patterns shown in Fig. 4 are obtained for SLP (Fig. S1) and 700-hPa wind and geopotential height (Fig. S2). At the 500-hPa level and above, the patterns are different.

Dynamical Interpretation of EOF2 of ISMR

EOF2 of ISMR, as defined in Fig. 2*B*, is characterized by negative ISMR anomalies over the Gangetic Plain and positive anomalies over peninsular India. The SST pattern observed in association with this pattern (Fig. 1 *C* and *E*), which is characterized by positive anomalies over the northern Arabian Sea and Bay of Bengal and the South China Sea, bears a strong

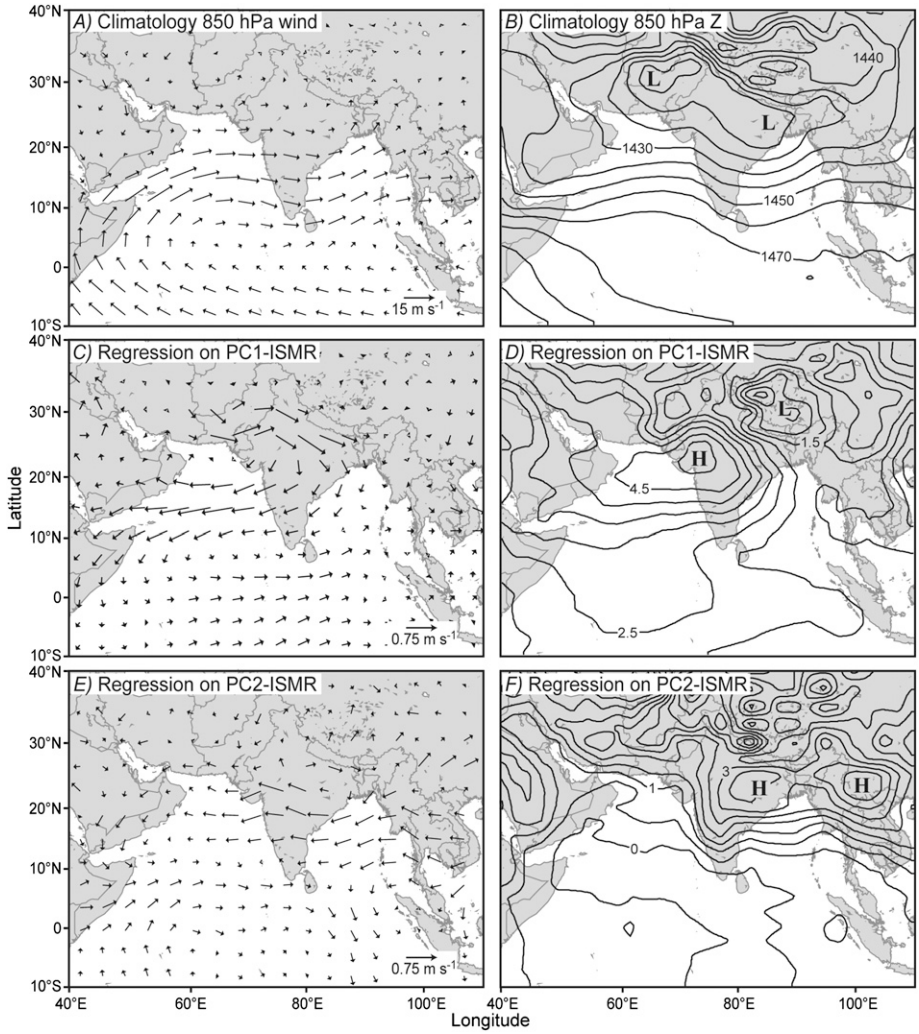

Fig. 4. Patterns of mean wind (meters per second) and geopotential height (meters) anomalies at 850-hPa level observed in association with EOF1 and EOF2 of ISMR (Fig. 2 *A* and *B*) based on data for 1958–2008. *A* and *B* show seasonally averaged (JJAS) climatological mean fields for wind and geopotential height (contour interval = 10 hPa). *C* and *D* show spatial patterns obtained by regressing the seasonally averaged wind and geopotential height fields on the standardized PC1 of ISMR. *E* and *F* are the same as *C* and *D* but for PC2. Wind vector scales in *A*, *C*, and *E* are located in the bottom right corner. Contour interval in *D* and *F* is 0.5 hPa.

resemblance to the lagged response to ENSO (Fig. 1*G*). The ISMR over the Gangetic plain and peninsular India exhibits a lagged response to ENSO (Fig. 1 *G* and *H*) that resembles the patterns derived from MCA (Fig. 1 *C*–*F*). It has been proposed that enhanced downward short-wave radiation and suppressed air sea fluxes of radiation and latent and sensible heat during El Niño events induce positive SST anomalies in the Indian Ocean that persist into the following JJAS (12). It can be inferred from Figs. 1 and 4 that summers after the peak of El Niño events tend to occur in association with a weakening of the westerlies over the northern Indian Ocean and the South China Sea (Fig. 4*E*), which should act to sustain the SST anomalies. However, it is not obvious why abnormal warmth of the northern Indian Ocean during these summers should favor suppressed monsoon rainfall over the Gangetic Plain. It seems more likely that the physical linkage between the ENSO cycle and ISMR rainfall anomalies in the subsequent summer is through the atmosphere.

Fluctuations in the amplitude and polarity of EOF2 of ISMR correspond to a strengthening and weakening of the monsoon trough over northern India (Fig. 4 *A* and *B*). A similar pattern of wind and geopotential height anomalies occurs on an intraseasonal time scale in association with the active and break phases of the monsoon, with the positive polarity of EOF2 being associated with the break phase (4–6, 17). The prominence of the monsoon trough is also closely related to the frequency of monsoon depressions that form over the Bay of Bengal and migrate west–northwestward across the Gangetic Plain over a period of a few days, bringing episodes of enhanced rainfall. Year-to-year variations in the relative prevalence of active and break phases of the monsoon and the number and strength of monsoon depressions occur naturally, even in the absence of SST anomalies. Hence, much of the year-to-year variability of EOF2 of ISMR can be interpreted as sampling fluctuations related to the intraseasonal variability, which is postulated in refs. 3–5.

Summary

In the text, we have shown the following four points:

(*i*) The first mode obtained by performing MCA on JJAS values of ISMR paired with the SST departure field over the Indian Ocean sector is nearly identical to the second mode derived from MCA of the same fields for a global SST domain. It describes the well-known relationship between ISMR averaged over India as a whole and the polarity of ENSO (i.e.,

the tendency for ISMR to be less, on average, during El Niño years than La Niña years). The second MCA mode, which is also consistent for the two SST departure field domains, is characterized by a dipole structure in ISMR (anomalies of opposing sign over the Gangetic Plain and peninsular India) paired with SST anomalies over the northern parts of the Arabian Sea and Bay of Bengal.

(*ii*) The two modes exhibit well-defined signatures in the low-level wind field over India. The first (ENSO-related) mode is mainly expressed in variations in the meridional wind component, and the second (dipole) mode mainly is expressed in the zonal wind component and the strength of the monsoon trough over northern India.

(*iii*) Both leading modes are ENSO-related; the first mode is observed concurrently with equatorial Pacific SST anomalies, and the second mode is, in part, a lagged response to ENSO.

(*iv*) Sampling fluctuations related to the intraseasonal variability of the ISMR and specifically, the cycling back and forth between active and break periods and the number and strength of monsoon depressions contribute to the year-to-year variability of EOF2.

Materials and Methods

Rainfall data over India used in this study are based on the University of Delaware monthly gridded precipitation data at 0.5° spatial resolution for the period from 1900 to 2008 (18) (version 2.01; http://www.esrl.noaa.gov/psd/data/gridded/data.UDel_AirT_Precip.html). For analysis of mean patterns for the summer monsoon season, the monthly mean data are averaged over the calendar months from July to September (JJAS). Data from the Global Precipitation Climatology Project (version 2.2), available on a 2.5° × 2.5° latitude/longitude grid from 1979 on and downloaded from http://www.esrl.noaa.gov/psd/data/gridded/data.gpcp.html, are used to extend the rainfall analysis over the Indian Ocean sector (30° S to 40° N, 40° E to 110° E) (19). Monthly SST data were obtained from the National Climatic Data Center's Extended Reconstructed Sea Surface Temperature (ERSST.v3b) at 2° spatial resolution for the period 1871–2010 (20, 21).

(*i*) The atmospheric fields are based on the European Centre for Medium-Range Weather Forecasts (ECMWF) Re-Analysis (ERA)-40 and ERA-interim data for the zonal and meridional wind components (*u* and *v*), SLP, temperature, and geopotential height at the 1,000-, 850-, 700-, 500-, and 300-hPa levels (22). The ERA-40 data for the period from 1957 to 2002 and the ERA-interim data for the period from 1989 to 2011 are merged and interpolated onto a common grid to form a continuous record from 1958 to 2008. For each of the selected variables from the reanalysis data, climatological means and anomalies are estimated for the monsoon season (JJAS).

(*ii*) MCA is performed to identify coupled patterns of monsoon season rainfall and SST departure field, obtained as described above, for the period from 1900 to 2008. A detailed description of MCA can be found in ref. 23, where it is referred to as singular value decomposition analysis. The period of analysis of the rainfall and SST data is 109 y (1900–2008).

(*iii*) EOF analysis of the monsoon season rainfall field for 1900–2008 is performed to identify the dominant modes of ISMR variability regardless of variations in other fields. The corresponding PCs are used as a basis for documenting the temporal and spatial variability in the rainfall field and its relation to the lower tropospheric circulation. The results are displayed in the form of regression or correlation maps, as indicated, between seasonal mean fields of a variable such as rainfall, wind, or geopotential height and one of the standardized PC time series.

To keep the displays simple, statistical significance is not displayed explicitly. However, for each of the regression maps, correlation maps were also generated, and in all cases, a Student *t* test applied to the correlation coefficients in the vicinity of the major centers of action was found to be significant at $P < 0.001$. The simplicity and dynamical consistency of the patterns also attest to their statistical significance, where *P* values are based on the conventional Student *t* test applied to the correlation coefficient.

ACKNOWLEDGMENTS. V.M. and D.P.L. were supported by the University of Washington's Robert and Irene Sylvester Endowment. B.V.S. and J.M.W. acknowledge the support of National Science Foundation Grant AGS-1122989.

1. Wahl ER, Morrill C (2010) Toward understanding and predicting monsoon patterns. *Science* 328:437–438.
2. Kumar KK, et al. (2010) The once and future pulse of Indian monsoonal climate. *Clim Dyn* 36:2159–2170.
3. Shukla J (1987) *Interannual Variability of Monsoons*, eds Fein JS, Stephens PL (Wiley, New York), pp 399–464.
4. Straus DM, Krishnamurthy V (2007) The preferred structure of the interannual Indian monsoon variability. *Pure Appl Geophys* 164:1717–1732.
5. Krishnamurthy V, Shukla J (2000) Intraseasonal and Interannual Variability of Rainfall over India. *J Clim* 13:4366–4377.
6. Krishnamurthy V, Shukla J (2008) Seasonal persistence and propagation of intraseasonal patterns over the Indian monsoon region. *Clim Dyn* 30:353–369.
7. Wainer I, Webster PJ (1996) Monsoon/El Nino-Southern Oscillation relationships in a simple coupled ocean-atmosphere model. *J Geophys Res* 101:25599–25614.
8. Kumar KK, Rajagopalan B, Cane MA (1999) On the weakening relationship between the Indian monsoon and ENSO. *Science* 284:2156–2159.
9. Rasmusson EM, Carpenter TH (1983) Relationship between eastern equatorial Pacific sea surface temperatures and rainfall over India and Sri Lanka. *Mon Weather Rev* 111: 517–528.
10. Saji NH, Goswami BN, Vinayachandran PN, Yamagata T (1999) A dipole mode in the tropical Indian Ocean. *Nature* 401:360–363.
11. Ashok K, Zhaoyong G, Saji NH, Yamagata T (2004) Individual and combined influences of ENSO and the Indian Ocean dipole on the Indian summer monsoon. *J Clim* 17: 3141–3155.
12. Klein SA, Soden BJ, Lau N-C (1999) Remote sea surface temperature variations during ENSO: Evidence for a tropical atmospheric bridge. *J Clim* 12:917–932.
13. Xie S-P, et al. (2009) Indian Ocean capacitor effect on Indo–Western Pacific climate during the summer following El Niño. *J Clim* 22:730–747.
14. Schott FA, Xie S-P, McCreary Jr. JP (2009) Indian Ocean circulation and climate variability. *Rev Geophys*, 10.1029/2007RG000245.
15. Parthasarathy B, Munot AA, Kothawale DR (1994) All-India monthly and seasonal rainfall series: 1871–1993. *Theor Appl Climatol* 49:217–224.
16. Walker GT (1924) Correlation in seasonal variations of weather, IX: Further study of world-weather (World Weather II). *Memoirs India Meteorol Dep* 24:275–332.
17. Manoj MG, Devara PCS, Safai PD, Goswami BN (2010) Absorbing aerosols facilitate transition of Indian monsoon breaks to active spells. *Clim Dyn* 37:2181–2198.
18. Legates DR, Willmott CJ (1990) Mean seasonal and spatial variability in gauge-corrected, global precipitation. *Int J Climatol* 10:111–127.
19. Adler RF, et al. (2009) The version-2 Global Precipitation Climatology Project (GPCP) monthly precipitation analysis (1979–present). *J Hydrometeorol* 4:1147–1167.
20. Smith TM, Reynolds RW, Peterson TC, Lawrimore J (2008) Improvements to NOAA's historical merged land-ocean surface temperature analysis (1880–2006). *J Clim* 21: 2283–2296.
21. Smith TM, Reynolds RW (2004) Improved extended reconstruction of SST (1854–1997). *J Clim* 17:2466–2477.
22. Dee D, et al. (2011) The ERA-Interim reanalysis: Configuration and performance of the data assimilation system. *Q J R Meteorol Soc* 137:553–597.
23. Bretherton CS, Smith C, Wallace JM (1992) An intercomparison of methods for finding coupled patterns in climate data. *J Clim* 5:541–560.